Biofunctionalized Hydrogel Microscaffolds Promote 3D Hepatic Sheet Morphology

Myung Hee Kim, Supriya K. Kumar, Hitomi Shirahama, Jeongeun Seo, Jae-Ho Lee, Vladimir P. Zhdanov, Nam-Joon Cho*

Development of artificial tissues providing the proper geometrical, mechanical, and environmental cues for cells is highly coveted in the field of tissue engineering. Recently, microfabrication strategies in combination with other chemistries have been utilized to capture the architectural complexity of intricate organs, such as the liver, in in vitro platforms. Here it is shown that a biofunctionalized poly (ethylene glycol) (PEG) hydrogel scaffold, fabricated using a sphere-template, facilitates hepatic sheet formation that follows the microscale patterns of the scaffold surface. The design takes advantage of the excellent diffusion properties of porous, uniform 3D hydrogel platforms, and the enhanced-cell–extracellular matrix interaction with the display of conjugated collagen type I, which in turn elicits favorable Huh-7.5 response. Collectively, the experimental findings and corresponding simulations demonstrate the importance of biofunctionalized porous scaffolds and indicate that the microscaffold shows promise in liver tissue engineering applications and provides distinct advantages over current cell sheet and hepatocyte spheroid technologies.

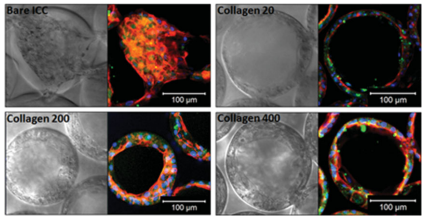

Dr. M. H. Kim, S. K. Kumar, H. Shirahama, Dr. J. Seo, Dr. J.-H. Lee, Prof. N.-J. Cho
School of Materials Science and Engineering
Nanyang Technological University
50 Nanyang Avenue, Singapore 639798, Singapore
E-mail: njcho@e.ntu.edu.sg
Dr. M. H. Kim, S. K. Kumar, H. Shirahama, Dr. J. Seo, Dr. J.-H. Lee, Prof. N.-J. Cho
Centre for Biomimetic Sensor Science
Nanyang Technological University
50 Nanyang Avenue, Singapore 639798, Singapore
Prof. V. P. Zhdanov
Boreskov Institute of Catalysis
Russian Academy of Sciences
Novosibirsk 630090, Russia
Prof. N.-J. Cho
School of Chemical and Biomedical Engineering
Nanyang Technological University
62 Nanyang Avenue, Singapore 637459, Singapore

1. Introduction

Microfabrication strategies enable the development of artificial tissues based on mimicking in vivo cellular environments, including geometrical, mechanical, and environmental cues along with efficient nutrient and waste transfer.[1–5] With emerging advances in 3D materials fabrication, there are new opportunities to design tissue engineering platforms that overcome the shortcomings of conventional 2D substrates.[6,7] As one of the most architecturally complex organs in the human body, the liver has motivated numerous 3D design strategies, including liver cell (or so-called hepatocyte) encapsulation within matrices,[8–10] spheroid culture,[11–14] sandwich hydrogels,[15,16] cell sheet engineering,[17–23] and macroporous scaffolds.[24] Based on the results obtained with various 3D platforms comprised of natural or synthetic biomaterials

© 2015 WILEY-VCH Verlag GmbH & Co. KGaA, Weinheim

DOI: 10.1002/mabi.201500338

as well as with rigid 2D polymeric substrates, there is general agreement that structural and functional properties of cultured hepatocytes more faithfully mimic the in vivo phenotype in 3D platforms.[25,26]

One of the most promising 3D scaffolds entails a microstructured hydrogel platform that provides hexagonally packed interconnected spherical cavities in order to promote cell aggregation and the formation of a cellular spheroid in each cavity, as demonstrated for hepatocytes and other cell types.[27–32] In order to create highly uniform microscale cavities for tunable spheroid size, the scaffold can be fabricated by inverted colloidal crystal (ICC) templating and utilizes nonfouling polymeric materials which minimize cell–scaffold interactions while taking advantage of the porous network for high mass transfer rates. Although the spheroid model is well accepted in liver tissue engineering,[33] there are high rates of necrosis at the spheroid core and accordingly motivation to develop new materials-inspired strategies to induce the formation of cell aggregates with different morphologies.

Herein, we report a new biofunctionalized hydrogel microscaffold that promotes hepatic sheet morphology with improved rates of cell viability and function. The recent advent of cell sheet technology and its growing success as a cell culture system reaffirm the importance of this aggregate morphology. In contrast to existing ICC-templated hydrogel scaffolds that promote weak-cell–scaffold interactions, our design involves the conjugation of Type I collagen (Col I)—which is known to bind to cell surface integrins and influence cell behavior—to the polymer scaffold, thereby establishing a bioactive platform that takes advantage of the diffusion properties of the 3D platform while facilitating the formation of sheet-like tissue architectures that follow the microscale patterns of the scaffold surface.

2. Research and Discussion

As the basis for our design strategy, we employ poly (ethylene glycol) diacrylate (PEG-DA) ICC scaffolds that are functionalized with chemically reactive acryloyl-PEG-NHS groups. Using standard EDC/NHS chemistry, these functional groups enable the covalent attachment of Col I to the scaffold surface with tunable protein coating densities. A schematic of the ICC fabrication and coating process is presented in Figure 1A. A major advantage of the ICC system is that the pore size and the size of necks between pores are controlled by the size of the porogen particles used, which in turn controls the size of the hepatocyte spheroids formed. We use 140 μm diameter polystyrene (PS) beads in order to not exceed the maximum penetration depth of oxygen (the diffusion limit of oxygen in tissue is around 150–200 μm[34]). Scanning electron microscopy (SEM) images of the scaffolds after particle leaching confirm the successful creation of aesthetically distinguished pore cavities with interconnectivities (Figure 1B). Quantification of the pore structure demonstrated a unimodal distribution of pore sizes with a mean diameter of 102.3 ± 9.3 μm (Figure 1C) and a mean interconnection diameter of 38.6 ± 4.3 μm (Figure 1D). Subsequent conjugation of Col I at concentrations of 20 μg mL^{-1} (Collagen 20), 200 μg mL^{-1} (Collagen 200), and 400 μg mL^{-1} (Collagen 400) resulted in thin uniform coatings along the surface of the hydrogel scaffolds, especially as the concentration of collagen increased (Figure 1E; Figure S1, Supporting Information). The topographical intricacies of the coated scaffolds imaged using SEM reveal an interwoven fiber mesh network on the scaffold surface, which is also more pronounced at higher collagen concentration (Figure 1F).

After verifying the intact and ordered ICC scaffolds with and without collagen coating, we next hosted human hepatocarcinoma cells (Huh-7.5) in the scaffolds as a model system in order to understand the effects of scaffold design on hepatocyte function. These cells were successfully cultured in the collagen-conjugated ICC scaffolds for a period of up to 2 weeks. Higher cell proliferation was observed when the cells were cultured in the bare 3D scaffolds compared to the 2D plate hepatocyte culture, as determined quantitatively by a cell counting assay kit (Figure 2A) and qualitatively by live/dead staining (Figure S2, Supporting Information). For the Collagen 200-coated scaffold, the proliferation of hosted cells was threefold higher and almost twofold higher than that of the 2D culture platform and the nonfunctionalized ICC scaffold, respectively. Further characterization of cell behavior using albumin ELISA demonstrated a positive correlation between collagen coating concentration and hepatocyte albumin secretion and a threefold increase in comparison to the nonfunctionalized ICC scaffold (Figure 2B).

Specific morphological differences observed through SEM images of the cell-laden scaffolds revealed that the cells aggregated form a spheroid in nonfunctionalized ICC scaffolds (Figure 2C), as shown in previous studies.[28,31,35] In stark contrast, the presence of the ECM coating redirects the assembly of hepatocytes into a channel where the cells are located primarily near the walls of the scaffold and form cell sheet-like aggregates aligning with the architecture of the scaffold. As the cells proliferate, they continue to line the walls of the cavities, and with this process of 3D self-assembled layering on the negatively curved surface the interconnections reach confluency by day 7.

To further characterize the cell-sheet-like assembly, we stained cells for albumin, F-actin, and nuclei, and

© 2015 WILEY-VCH Verlag GmbH & Co. KGaA, Weinheim

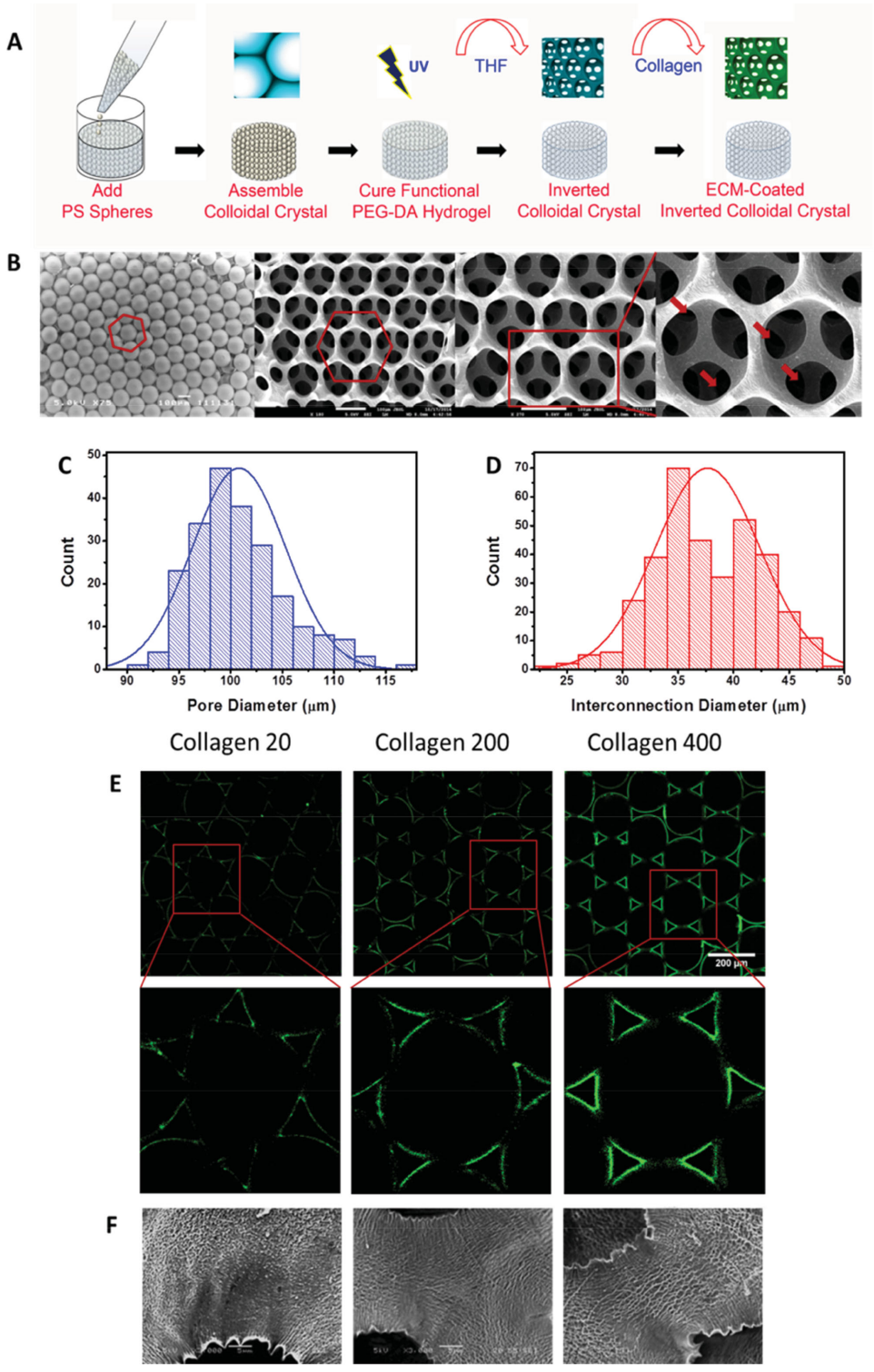

Figure 1. PEG-DA hydrogel scaffold fabrication by ICC templating and Col I-functionalization. A) Schematic illustrating the fabrication process of ICC scaffolds. B) SEM micrographs of colloidal crystals made from 140 μm polystyrene beads (left) and ICC scaffold at different magnification. Red arrows point to the interconnections between pores. Analysis of the SEM micrograph by ImageJ allowed histogram construction of C) pore and D) interconnection diameters. The ICC hydrogels were freeze-dried before imaging, resulting in the shrinkage of the pore and interconnection diameters. E) Confocal microscopy images of the ICC scaffolds after functionalization with different concentrations of Col I (20, 200, and 400 μg mL^{-1}). Col I was stained with a specific Col I antibody (green). F) SEM images of ICC scaffold coating with collagen, after dehydration process, showed collagen fibril in a dose dependent manner. Scale bars are B) 100 μm, E) 200 μm, and F) 5 μm.

© 2015 WILEY-VCH Verlag GmbH & Co. KGaA, Weinheim
Materials Views
www.MaterialsViews.com

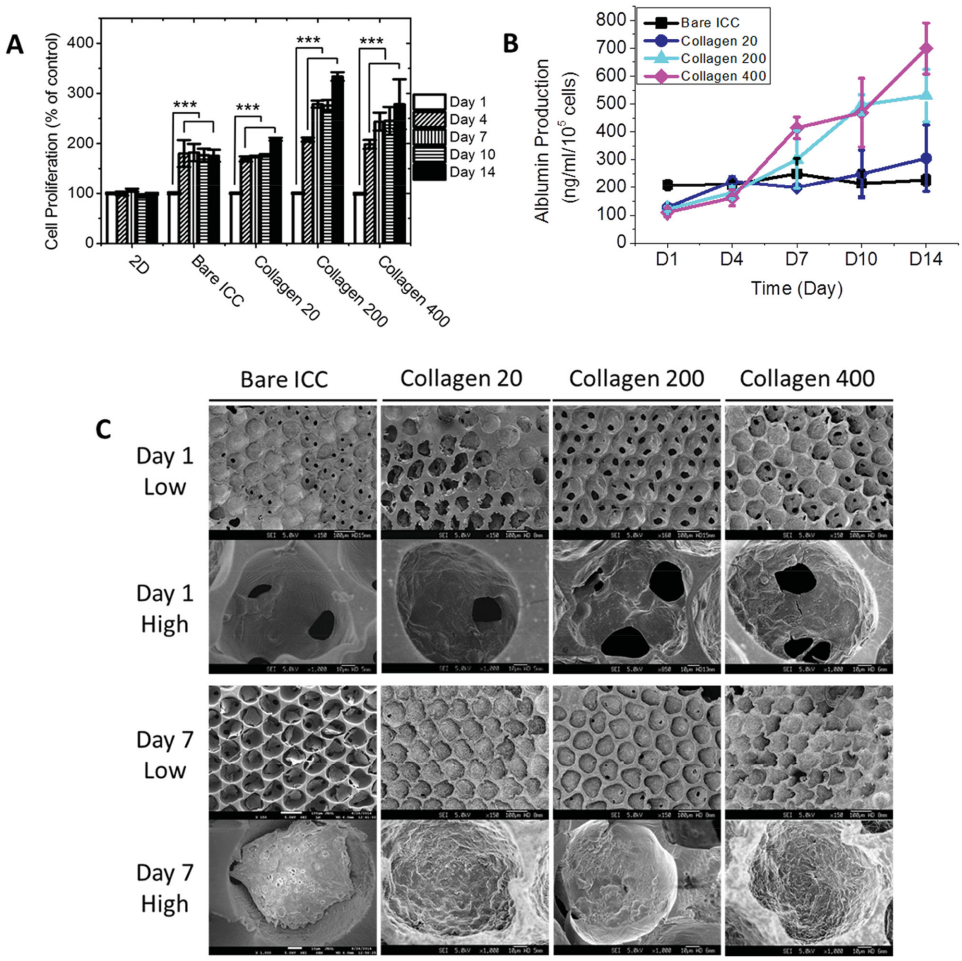

Figure 2. Evaluation of Huh-7.5 cell proliferation, function, and attachment pattern in 3D ICC scaffolds. Huh-7.5 cells (10^6) were seeded in 2D culture plates or 3D ICC scaffolds coated with or without collagen. After cell seeding on Day 0, A) cell proliferation was quantified by CCK-8 colorimetric assay on days 1, 4, 7, 10, and 14. The data were normalized to Day 1 absorbance values and then converted into percentages of the control ($n = 3$, mean ± SD; ***: $p < 0.001$ versus day 1 each group). B) Albumin secretion was detected from collected media samples, on the days indicated above, using human albumin ELISA. Albumin secretion was normalized by cell number according to cell metabolism rate. C) SEM micrographs of cell-laden ICC scaffolds with different concentrations of Col I on day 1 and day 7 (scale bars 100 μm and 10 μm for low and high magnification, respectively) were taken after fixation and dehydration, indicating the different cell growth patterns.

imaged them using confocal microscopy (Figure S4, Supporting Information). In accordance with the SEM images, the immunofluorescent images confirmed that nonfunctionalized ICC scaffolds support spheroid formation (Figure 3A) while the collagen-coated scaffolds promote formation of 3D sheet-like cell aggregates. Quantification of the multilayer cell sheet thickness demonstrated that cells could self-assemble into up to three cell layers (≈27 μm thick) by day 14 (Figure 3B).[20] The dramatic alteration of morphology in the collagen-coated ICC scaffolds and the enhanced albumin secretion by the Huh-7.5 cells demonstrate the functional importance of the improved cell-ECM and cell–cell interactions.

To investigate the underlying molecular mechanism behind the multilayer cell sheet phenomenon observed in the Col I-functionalized hydrogel scaffolds, we analyzed the gene expression profile for three adhesion proteins using real time PCR: integrin β1, E-cadherin, and N-cadherin. Integrins are a large family of proteins that function to link the cells and the ECM proteins.[36] In the case of α5β1-integrin and collagen, integrin-ECM mediated cell contacts have been shown to regulate spheroid formation.[37] E-cadherin plays a vital role in mediating cell–cell adhesion in several cell types, including primary hepatocytes.[38] Importantly, we observed that E-cadherin was the major adhesion molecule expressed in a collagen dose-dependent and time-dependent manner in our system (Figure S4A, Supporting Information). In the Collagen 400-coated ICC scaffolds, E-cadherin was highly upregulated in comparison to the nonfunctionalized ICC group on day 14 (≈fourfold), which suggests an increased level of homotypic cell interactions in the multilayer

© 2015 WILEY-VCH Verlag GmbH & Co. KGaA, Weinheim

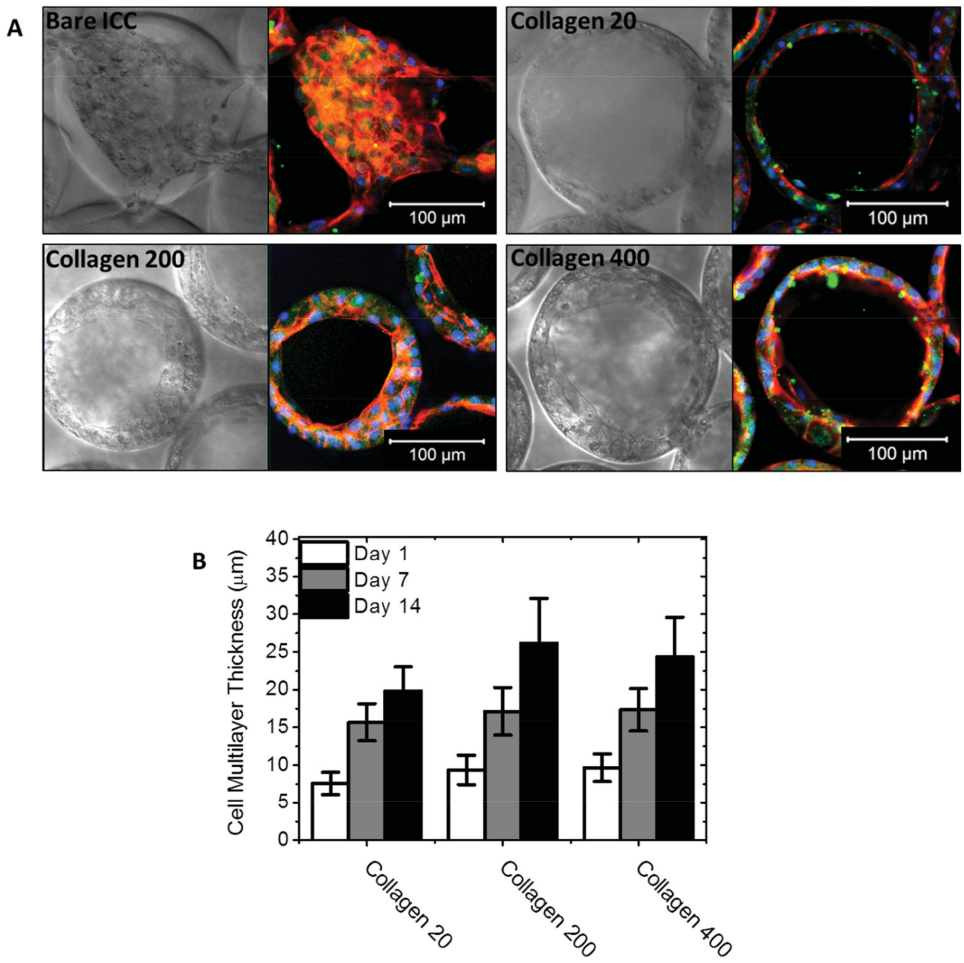

Figure 3. Characterization of hepatic multilayer sheet formation in 3D ICC scaffold depending on the collagen concentration and the culture time period. A) DIC and immunofluorescent images of Huh-7.5 cells on day 14, taken by confocal microscopy, showed the multilayer sheets formed by the cells. Albumin (green) was stained by Alexa Fluor 488-conjugated second antibody, f-actin (red) was stained by Alexa Fluor 555-labeled phalloidin, and nuclei (blue) were counterstained by DAPI. B) Cell multilayer thickness was quantified by analyzing the confocal images with ImageJ. The thickness of five points on each image was measured and averaged ($n = 3$).

assembly. The gene expression levels of N-cadherin (Figure S4B, Supporting Information) and Integrin β1 (Figure S4C, Supporting Information) were slightly upregulated by the presence of higher doses of collagen (Collagen 200 and Collagen 400), indicating the role of cell–ECM interactions in the hydrogel scaffold.

Based on the experimental evidence, we employed 2D Monte Carlo (MC) simulations of cell proliferation in two adjacent cavities connected by a neck (Figure 4; for the details, see Section 3 in the Supporting Information) in order to illustrate the role of cell–cell and cell–scaffold adhesion in cell aggregation and to clarify how this process can influence the connectivity of pores. If cell–surface adhesion is negligible or weak (e.g., nonfunctionalized ICC), then cell proliferation results in cell aggregation and spheroid formation in the center of the cavities. On the other hand, if cell–surface adhesion is moderate or strong (e.g., ECM-coated ICC), then cell aggregation and growth occurs primarily near the scaffold surface, leading to multilayer hepatocyte sheet formation. These simulations yield excellent agreement with the experimental findings and further support that the ECM functionalization promotes hepatic-like sheet formation through induction of strong cell–surface adhesion. A comparative strategic schematic of the hepatocyte spheroid and multilayer hepatocyte sheet formation in the absence and presence of an ECM coating is presented in Figure S5 in the Supporting Information.

Irrespective whether cells are aggregated as spheres or sheets, their location is nearly close-packed, and the mass transport in the space between cells is inefficient. With increasing hepatosphere size above 200–400 μm, the cell proliferation can accordingly be limited or terminated by the supply of oxygen and nutrients and removal of metabolites.[31] In our scaffolds, the size of aggregates restricted by the size of cavities is smaller. In this case,

© 2015 WILEY-VCH Verlag GmbH & Co. KGaA, Weinheim

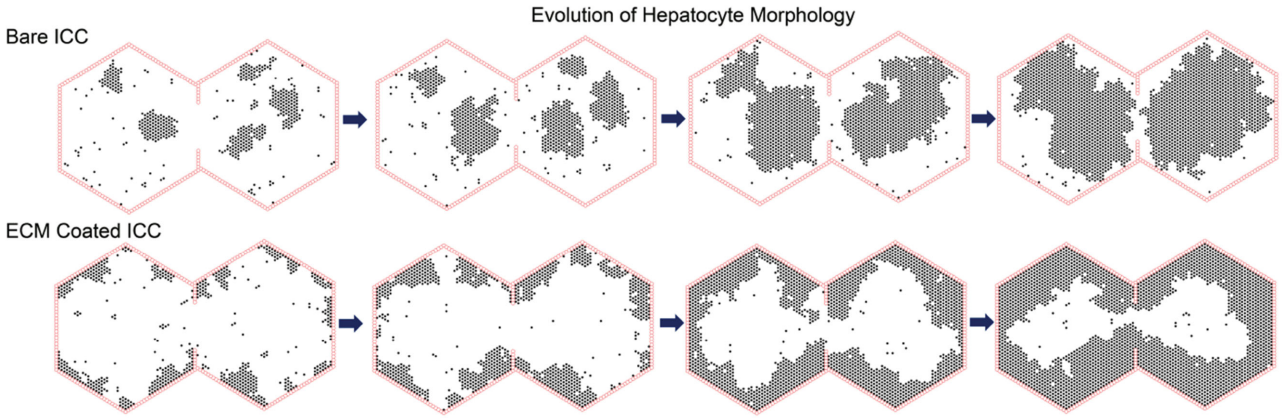

Figure 4. Representative lattice snapshots during MC simulations of cell proliferation in two adjacent cavities connected by a neck. The cavities are mimicked by hexagons. The boundary sites shown by open squares represent the scaffold surface. Cells are exhibited by filled circles. Two series of snapshots correspond to the bare ICC and ECM-coated ICC scaffolds, respectively. The fractions of occupied sites in each series are 0.1, 0.2, 0.4, and 0.6.

the supply of oxygen and/or nutrient can, however, be limited at the level of a scaffold, i.e., there is critical scaffold size. Our analysis, based on the conventional reaction–diffusion equations (Section 4, Supporting Information), indicates that the critical scaffold size is about 0.5 cm, a value larger than the size of our scaffold (0.2 cm). Thus, the mass-transport limitations are not significant in our case, but should receive attention if the scaffold size is increased depending on application needs.

3. Conclusion

In conclusion, we have developed a novel biomaterials platform that directs the multilayer sheet assembly of hepatocytes within an ICC-templated hydrogel scaffold. We were able to control the coating density of Col I protein on the surface of the PEG scaffold, which in turn allowed enhanced cell–cell and cell–ECM interactions. The facile microfabrication techniques and simple chemistries employed here to facilitate this cell sheet morphology prove more advantageous than existing cell sheet complicated technologies and hepatocyte spheroid platforms. We confirmed the dependence of the cell morphology on the adhesion properties of the scaffold by Monte Carlo simulations and clarified analytically the likely changes in the cell behavior due to mass-transport limitations in bare and ECM-coated scaffolds. This treatment helps to understand the limitations on the size of the whole scaffold. In a broader context, the ECM-conjugated porous scaffold can be employed for different cell types and can be easily tethered with different compositions of ECM proteins with the eventual goal to fabricate clinically applicable tissues for use in tissue regeneration, transplantation, xenobiotic toxicity testing, and liver disease studies. Taken together, we demonstrate that materials fabrication strategies can be employed to tune the adhesive properties of the scaffold, thereby enabling control over cell proliferation and aggregation.

4. Experimental Section

Synthesis of PEGDA: PEGDA (M_W = 4600) was synthesized as previously described.[39] Briefly, diol-terminated PEG (M_W = 4600; Sigma) reacted with a 2.5 mol excess of acryloyl chloride and triethylamine base catalyst in tetrahydrofuran (THF; Sigma) overnight at room temperature. The collected PEGDA was then purified by filtration, liquid–liquid extraction in dichloromethane, and precipitation in diethyl ether.

Preparation of Colloidal Crystal Lattices: Polystyrene (PS) spheres (D =140 μm; Duke Scientific Corporation) were pipetted into Eppendorf tube molds and washed with 70% ethanol (Merck). The assemblies were placed in an ultrasonic bath to arrange the spheres into ordered crystal colloidals (CCs). PS spheres were annealed in a furnace at 130 °C for 6 h.

Preparation of Prepolymer Solution: To prepare the PEGDA solution for scaffolds without a collagen coating, 50% (w/v) PEGDA and 0.05% (w/v) Irgacure 2959 (I2959, Sigma) were dissolved in deionized water. Similarly, the PEGDA-PEG-NHS prepolymer solution for scaffolds with a collagen coating was prepared by thoroughly mixing 50% (w/w) PEGDA, 10% (w/v) acryloyl-PEG-NHS (PEG-NHS; Laysan Bio, Inc.), and 0.05% (w/v) I2959 in deionized water.

Fabrication and Characterization of Inverted Colloidal Crystal (ICC) Scaffolds: The prepolymer solution infiltrated the annealed colloidal crystal by centrifugation for 5 min and excess precursor solution was removed by blotting. PEGDA and ICC was then exposed to 365 nm UV light (Bluewave 200 UV spotlight, Blaze Technology) at 10.84 mW cm^{-2} for 5 min for polymerization. The hydrogel and CC complex were then soaked in THF for 24 h to dissolve PS spheres completely. ICC scaffolds were washed with phosphate buffered saline (PBS; Hyclone) for at least 4 h and ICCs containing PEG-NHS were coated in collagen I solution (from rat tail; Sigma) by centrifugation and shaking for 30 min and then

© 2015 WILEY-VCH Verlag GmbH & Co. KGaA, Weinheim

stored at 4 °C overnight. The ICC scaffolds were sterilized by ultraviolet (UV) light for 30 min before cell culture use.

Preparation of Scaffolds for SEM: ICC scaffolds were first fixed with 4% Paraformaldehyde (PFA; Alfa Aesar) and then transferred sequentially to 25%, 50%, 75%, 95%, and 100% ethanol for 30 min each and to make sure of proper water removal. The scaffolds were stored at −80 °C until ethanol evaporated completely and then dried in a freezone 4.5 (Lobconco) freeze drier for 48 h. The SEM samples were coated with a Pt film of 10 nm thickness using a JFC-1600 (JEOL) sputter coater and the micrographs were taken with a JSM-7600F (JEOL) FE-SEM instrument at a voltage of 5 kV.

Cell Culture: Human hepatocarcinoma cells (Huh-7.5; Apath) were maintained in Dulbecco's modified Eagle's medium (DMEM; Hyclone) supplemented with 10% fetal bovine serum (FBS; Hyclone), 100 U mL^{-1} penicillin (Life Technologies), and 100 mg mL^{-1} streptomycin (Life Technologies) in a humidified atmosphere with 5% CO_2 at 37 °C. Medium was changed every 3 d before cell seeding for 3D cell culture. For cell seeding, the ICC scaffolds were placed and washed with PBS in 24-well plates (Corning), and kept in 2 mL complete media for 30 min. Media were aspirated and scaffolds were dried for 1 h under UV light for sterilization. Cells were detached from the culture plate using 0.25% Trypsin-EDTA solution (Life Technologies) and collected cells were adjusted to 4×10^7 cells in 1 mL media. A 25 μL volume containing 1×10^6 cells was carefully pipetted on top of each ICC scaffold. After 12 h, cell-seeded ICC scaffolds were transferred into new 24-well plates and media was changed every 3 d.

Viability and Proliferation Assays of Huh-7.5 within the ICC Scaffold: The cell viability in ICC scaffolds was measured using the LIVE/DEAD Cell Viability/Cytotoxicity kit (Life Technologies) according to manufacturer's protocol. In brief, 4 μM calcein-AM and 8 μM ethidium homodimer-1s (EthD-1) were prepared in complete media and added to the cell-laden scaffold and incubated at 37 °C. After incubation for 1 h, live cells stained by Calcein-AM were imaged as green using a 494–517 nm emission filter, and dead cells stained by EthD-1 were imaged as red using a 517–617 nm emission filter by confocal microscope (LSM710, Carl Zeiss) under a laser excitation of 488 nm. Cell proliferation in ICCs was analyzed quantitatively using Cell Counting Kit-8 (CCK-8; Dojindo Molecular Technologies) according to the manufacturer's instructions. Typically, after cells were incubated with CCK-8 for 1 h at 37 °C, the colorimetric culture media were measured with a plate reader using a 450 nm wavelength. Measured absorbance was converted to cell number with a standard curve. The experiment was repeated three times.

Function Assays of Huh-7.5 within the ICC Scaffold: Aliquots of media from cell cultures of the ICC scaffold were collected every 3 d, debris was removed by centrifugation, and the supernatants were stored at −20 °C. Albumin concentration was determined using a human albumin enzyme-linked immunosorbent assay (ELISA) kit (Abcam) according to the manufacturer's instructions. The experiment was performed three times, and the data for the parameters were normalized against the cell number and amount of albumin on Day 1.

The transcript levels of regulative and functional genes in 3D ICC hydrogel cultures were determined at various time points after cell seeding. Primers were chosen with an online primer design program;[40] primer nucleotide sequences are presented in Table S1 (Supporting Information). Isolation of total RNA, synthesis of cDNA, and quantitative real-time PCR were carried out as described previously.[41] In brief, total RNA was isolated with TRIzol reagent (Life Technologies), followed by the synthesis of the first strand cDNA with iScript Reverse Transcription Supermix (Bio-Rad Laboratories). Next, SYBR green-based real-time quantitative PCR (qPCR) was performed with the SYBR select Master Mix for CFX (Life Technology) in the CFX connect real-time PCR system using amplification mode (95 °C for 20 s, followed by 40 cycles of 10 s at 95 °C, and 40 s at 60 °C). All reactions were run three times, and data were analyzed by the $2^{-\Delta\Delta CT}$ method, as described previously.[42] The values were normalized against the input determined for the housekeeping gene, glyceraldehyde 3-phosphate dehydrogenase (GAPDH).

Immunostaining and Confocal Microscopy: Cell-laden ICC scaffolds were collected at various time points for immunocytochemistry. Cells were washed twice with PBS, fixed with 4% PFA for 5 min, permeabilized with 0.1% Triton X-100 in PBS for 30 min, washed again with PBS and incubated in a 3% BSA blocking buffer in PBS for 1 h. The CYP3A4 and albumin were stained with specific primary antibody (Santa Cruz Biotechnology) overnight at 4 °C and then washed three times with PBS to remove unbound primary antibody. The cells were incubated with anti-mouse secondary antibody conjugated with Alexa Fluor 488 (Life Technologies). At the same time, filamentous actin (F-actin) was stained with Alexa Fluor 555 labeled phalloidin (Life Technologies) for 2 h at room temperature. After washing twice with PBS, nuclei were stained with 10 μg mL^{-1} 2,6-diamidino-2-phenylinodole, dihydrochloride (DAPI; Life Technologies) for 5 min. Stained cell images were captured with a confocal microscope, LSM710 with a ZEN program (Carl Zeiss).

Statistical Analysis: The significance of differences between the groups was studied using the paired two-tailed Student's *t*-test. Significance of gene expression was determined using GAPDH-normalized $2^{-\Delta\Delta CT}$ values. All data are represented as means ± SD. *, $p < 0.05$; **, $p < 0.01$; ***, $p < 0.001$.

Supporting Information

Supporting Information is available from the Wiley Online Library or from the author.

Acknowledgements: The authors wish to acknowledge support from a National Research Foundation Fellowship (NRF -NRFF2011-01) and Competitive Research Programme (NRF-CRP10-2012-07).

Received: September 8, 2015; Revised: October 7, 2015; Published online: November 27, 2015; DOI: 10.1002/mabi.201500338

Keywords: biofunctionalization; cellular adhesion; liver tissue engineering; microfabrication; poly (ethylene glycol) (PEG) hydrogels

[1] L. G. Griffith, G. Naughton, *Science* **2002**, *295*, 1009.
[2] A. Khademhosseini, R. Langer, J. Borenstein, J. P. Vacanti, *Proc. Natl. Acad. Sci. USA* **2006**, *103*, 2480.
[3] H. Andersson, A. Van Den Berg, *Lab Chip* **2004**, *4*, 98.

© 2015 WILEY-VCH Verlag GmbH & Co. KGaA, Weinheim

[4] A. Khademhosseini, R. Langer, *Biomaterials* **2007**, *28*, 5087.
[5] D. Yoon No, K.-H. Lee, J. Lee, S.-H. Lee, *Lab Chip* **2015**.
[6] J. Lee, M. J. Cuddihy, N. A. Kotov, *Tissue Eng. Part B* **2008**, *14*, 61.
[7] D. Sullivan, J. Repper, A. Frock, P. McFetridge, B. Petersen, *Curr. Pathobiol. Rep.* **2015**, *3*, 99.
[8] M. Kim, J. Y. Lee, C. N. Jones, A. Revzin, G. Tae, *Biomaterials* **2010**, *31*, 3596.
[9] C. Y. Li, K. R. Stevens, R. E. Schwartz, B. S. Alejandro, J. H. Huang, S. N. Bhatia, *Tissue Eng. Part A* **2014**.
[10] K. R. Stevens, J. S. Miller, B. L. Blakely, C. S. Chen, S. N. Bhatia, *J. Biomed. Mater. Res. Part A* **2015**.
[11] J. Pollok, D. Kluth, R. Cusick, H. Lee, H. Utsunomiya, P. Ma, R. Langer, C. Broelsch, J. Vacanti, *Eur. J. Pediatr. Surg.* **1998**, *8*, 195.
[12] A. Ananthanarayanan, B. Nugraha, M. Triyatni, S. Hart, S. Sankuratri, H. Yu, *Mol. Pharma.* **2014**, *11*, 2106.
[13] P. J. O'Brien, W. Luo, D. Rogozhnikov, J. Chen, M. N. Yousaf, *Bioconjugate Chem.* **2015**.
[14] Y. Liu, L. Zhang, J. Wei, S. Yan, J. Yu, X. Li, *J. Mater. Chem. B* **2014**, *2*, 3029.
[15] E. L. LeCluyse, A. Madan, G. Hamilton, K. Carroll, R. DeHaan, A. Parkinson, *J. Biochem. Mol. Toxicol.* **2000**, *14*, 177.
[16] M. Hegde, R. Jindal, A. Bhushan, S. Bale, W. Mccarty, I. Golberg, B. Usta, M. L. Yarmush, *Lab Chip* **2014**.
[17] Y. Tsuda, A. Kikuchi, M. Yamato, G. Chen, T. Okano, *Biochem. Biophys. Res. Commun.* **2006**, *348*, 937.
[18] Y. Tsuda, T. Shimizu, M. Yamato, A. Kikuchi, T. Sasagawa, S. Sekiya, J. Kobayashi, G. Chen, T. Okano, *Biomaterials* **2007**, *28*, 4939.
[19] M. Matsusaki, K. Kadowaki, Y. Nakahara, M. Akashi, *Angew. Chem.* **2007**, *119*, 4773.
[20] F. Evenou, T. Fujii, Y. Sakai, *Tissue Eng. Part C* **2010**, *16*, 311.
[21] Z. Baimakhanov, K. Yamanouchi, Y. Sakai, M. Koike, A. Soyama, M. Hidaka, M. Takatsuki, F. Fujita, K. Kanetaka, T. Kuroki, S. Eguchi, *Cell Transplant* **2015**.
[22] K. Kim, K. Ohashi, R. Utoh, K. Kano, T. Okano, *Biomaterials* **2012**, *33*, 1406.
[23] K. Ohashi, T. Yokoyama, M. Yamato, H. Kuge, H. Kanehiro, M. Tsutsumi, T. Amanuma, H. Iwata, J. Yang, T. Okano, Y. Nakajima, *Nat. Med.* **2007**, *13*, 880.
[24] A. Tripathi, J. S. Melo, *RSC Adv.* **2015**, *5*, 30701.
[25] A. Lazar, H. J. Mann, R. P. Remmel, R. A. Shatford, F. B. Cerra, W.-S. Hu, *In Vitro Cell. Dev. Biol. Anim.* **1995**, *31*, 340.
[26] T. T. Chang, M. Hughes-Fulford, *Tissue Eng. Part A* **2008**, *15*, 559.
[27] M. J. Cuddihy, N. A. Kotov, *Tissue Eng. Part A* **2008**, *14*, 1639.
[28] N. A. Kotov, Y. Liu, S. Wang, C. Cumming, M. Eghtedari, G. Vargas, M. Motamedi, J. Nichols, J. Cortiella, *Langmuir* **2004**, *20*, 7887.
[29] Y.-C. Kuo, K.-H. Chiu, *Biomaterials* **2011**, *32*, 819.
[30] Y.-C. Kuo, Y.-T. Tsai, *Biomacromolecules* **2010**, *11*, 731.
[31] J. Lee, M. J. Cuddihy, G. M. Cater, N. A. Kotov, *Biomaterials* **2009**, *30*, 4687.
[32] T. J. Long, C. C. Sprenger, S. R. Plymate, B. D. Ratner, *Biomaterials* **2014**, *35*, 8164.
[33] R. Z. Lin, H. Y. Chang, *Biotechnol. J.* **2008**, *3*, 1172.
[34] A. L. Harris, *Nat. Rev. Cancer* **2002**, *2*, 38.
[35] Y. Zhang, S. Wang, M. Eghtedari, M. Motamedi, N. A. Kotov, *Adv. Funct. Mater.* **2005**, *15*, 725.
[36] W. Guo, F. G. Giancotti, *Nat. Rev. Mol. Cell Biol.* **2004**, *5*, 816.
[37] R. C. Casey, K. M. Burleson, K. M. Skubitz, S. E. Pambuccian, T. R. Oegema, L. E. Ruff, A. P. Skubitz, *Am. J. Pathol.* **2001**, *159*, 2071.
[38] R. Narayanan, A. Rink, C. W. Beattie, W.-S. Hu, *Mamm. Genome* **2002**, *13*, 515.
[39] D. J. Waters, K. Engberg, R. Parke-Houben, L. Hartmann, C. N. Ta, M. F. Toney, C. W. Frank, *Macromolecules* **2010**, *43*, 6861.
[40] S. Rozen, H. Skaletsky, *Methods Mol. Biol.* **2000**, *132*, 365.
[41] S. Jeong, M. Rebeiz, P. Andolfatto, T. Werner, J. True, S. B. Carroll, *Cell* **2008**, *132*, 783.
[42] K. J. Livak, T. D. Schmittgen, *Methods* **2001**, *25*, 402.

© 2015 WILEY-VCH Verlag GmbH & Co. KGaA, Weinheim